Materials & Design 232 (2023) 112092

Contents lists available at ScienceDirect

Materials & Design

journal homepage: www.elsevier.com/locate/matdes

Multiscale characterization and modeling of aggregate contact effects on asphalt concrete's tension–compression asymmetry

Zhifei Tan [a,b], Bin Yang [a,b], Zhen Leng [a,b,*], Denis Jelagin [c,*], Peng Cao [d], Rui Li [a,b,e], Fuliao Zou [a,b]

[a] Department of Civil and Environmental Engineering, The Hong Kong Polytechnic University, Hong Kong, China
[b] Research Center for Resources Engineering Towards Carbon Neutrality, The Hong Kong Polytechnic University, Hong Kong, China
[c] Department of Civil and Architectural Engineering, KTH Royal Institute of Technology, Brinellvägen 23, 10044 Stockholm, Sweden
[d] College of Architecture and Civil Engineering, Beijing University of Technology, Beijing, China
[e] National & Local Joint Engineering Research Center of Transportation and Civil Engineering Materials, Chongqing Jiaotong University, Chongqing, China

HIGHLIGHTS

- AC's tension–compression (TC) asymmetry was characterized through multiscale tests and modeling.
- Due to the unique microscale contact characteristics, the contact region (CR) shows significant TC asymmetry.
- This microscale asymmetry further leads to the macroscale asymmetry of asphalt concrete (AC).

GRAPHICAL ABSTRACT

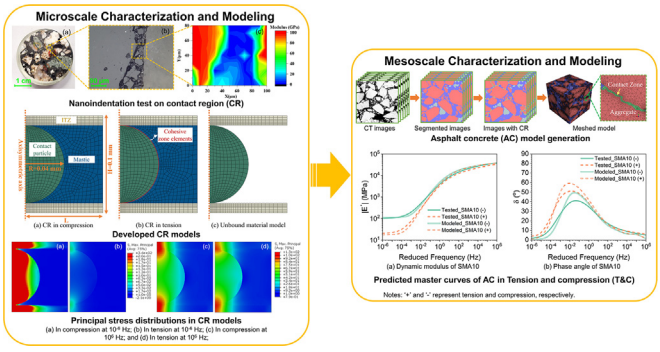

ARTICLE INFO

Article history:
Received 9 January 2023
Revised 29 April 2023
Accepted 11 June 2023
Available online 14 June 2023

Keywords:
Tension-compression asymmetry
Aggregate contacts
Contact region
Finite element analysis

ABSTRACT

Asphalt concrete (AC) exhibits significant tension–compression (TC) asymmetry and aggregate contacts can be one of the critical contributors to this behavior. Nevertheless, the underlying mechanisms are still unclear, and there has been no study to quantify this behavior. To fill the research gap, multiscale characterization and modeling on AC were performed in this study. At the microscale level, nanoindentation tests were conducted to characterize the aggregate contact characteristics in the contact region (CR). The CR was found to have a sandwich-like structure consisting of two interfacial layers, large filler particles, and asphalt mastic. Accordingly, micromechanical models of CR were developed to predict its mechanical behavior in tension and compresison (T&C). The modeling results showed that aggregate contacts significantly increase the compressive modulus, leading to the substantial TC asymmetry of CR. The predicted viscoelastic properties of CR were further applied to the developed mesostructural model of AC. The predicted master curves in T&C showed significant asymmetry and quantitatively agreed with the experimental ones, demonstrating the effectiveness of the adopted modeling approaches. This study is the first study to quantify the asymmetric performance of AC. The outcomes can be applied to evaluate AC's TC asymmetry effects on pavement performance.

1. Introduction

Asphalt concrete (AC) is a composite granular material composed of asphalt binder, a large proportion of aggregates, and air

* Corresponding authors at: Department of Civil and Environmental Engineering, The Hong Kong Polytechnic University, Hong Kong, China (Z. Leng).
E-mail addresses: zhen.leng@polyu.edu.hk (Z. Leng), denis.jelagin@abe.kth.se (D. Jelagin).

https://doi.org/10.1016/j.matdes.2023.112092
0264-1275/

voids. Due to the substantial heterogeneity in its compositions and microstructures, AC exhibits complicated mechanical performance under external load. At a small strain level, AC performs as a linear viscoelastic (LVE) material, where the deformation is completely recoverable [1–3]. Hence, the dynamic modulus of AC is generally characterized and used as one of the primary parameters in the mechanistic-empirical pavement design guide (MEPDG) [4]. At medium strain levels, irrecoverable deformation appears, and AC is described by the viscoplastic constitutive theories [5–7]. With further increasing strains, damage may be incurred in AC, and accordingly, damage theories may be applied [8–11]. Although significant efforts have been made in the past, it is still common to assume AC mixture as an isotropic viscoelastic-viscoplastic material due to the complexity of its performance.

Nevertheless, what is unexpected is that significant asymmetry has been observed at a small strain level (<200 με) in many previous studies [12–16]. Particularly, AC performs direction-dependent and exhibits much higher stiffness in compression than in tension [15,17–20]. In an earlier study, at 20 °C, AC's compressive modulus was one to two times higher than the tensile modulus [21]. Even a ten-time difference in compressive and tensile strengths has been reported [22]. Besides, this discrepancy is more prominent at a higher temperature [13,20]. At intermediate and high temperatures, 2.5 and 4 times higher compressive moduli were observed [23].

Although this tension-compression (TC) asymmetry has been broadly observed in many studies, its underlying mechanisms are still unclear. Research showed that this asymmetric performance could be ascribed to AC's heterogeneous structure [24–27]. As illustrated in Fig. 1, it has been speculated that in tension and compression (T&C), the aggregate structure was pulled apart and pushed closer, respectively, and thus AC reflected more the response of the asphalt matrix in tension and aggregates in compression [23–25]. This speculation gives a phenomenological explanation but cannot reveal the underlying mechanisms.

Research on analytical micromechanical modeling of AC provides a deeper insight into its mechanisms. Previous studies showed that the analytical micromechanical models generally underestimated the moduli of AC, especially at low frequencies [26–28]. The lack of consideration of aggregate contacts, i.e., the interactions of the aggregates in close proximity [30–32], was assumed to be the cause of this underestimation [29,30]. In compression, rather than transmitting the stress through the weak asphalt matrix, the rigid aggregate contacts may significantly improve the stress transmission efficiency between aggregates and thus enhance the stiffness of AC [1]. In contrast, the absence of aggregate contacts in tension leads to a lower modulus. More recently, a few studies considered aggregate contacts in the analytical micromechanical model by introducing contact parameters [29,30,33,34]. Significant improvement in the predicted moduli was observed. However, the analytical method is generally applied to simple structures and only provides a qualitative prediction. To understand how aggregate contacts affect the performance of AC in T&C, detailed microstructural properties should be incorporated into the modeling.

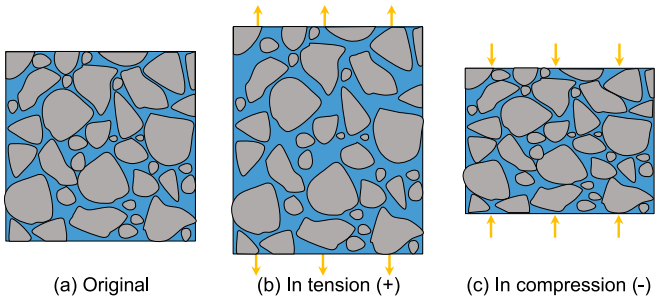

Fig. 1. Schematic diagram of AC in T&C.

Numerical micromechanical modeling may be an alternative solution to this problem [35]. In the modeling, the simulation is performed on the developed microstructural or mesostructural model through numerical methods, such as finite element (FE) and discrete element (DE) methods [36–38]. By considering more detailed microstructural properties in the developed microstructural model, numerical modeling can often offer much more accurate predictions than analytical methods. In addition to the macro properties, the local stress/strain can also be obtained from numerical modeling. However, introducing detailed microstructural properties may significantly complicate the model of AC and even make it computationally impossible. Multiscale modeling may be a solution to this issue. Instead of considering all microstructural properties in one model, the microstructural properties are hierarchically introduced into the models at different length scales. Thus, the computational cost at each scale can be significantly reduced. At the mesoscale, AC is commonly regarded as a composite material composed of aggregate, matrix, and air voids. One additional component, contact region (CR), may be incorporated to bridge the microscale aggregate contact characteristics with the mesoscale AC in the multiscale modeling. Here, CR is defined as the proximate area between the neighboring aggregates [1]. It can be captured by the surface distance threshold (SDT), which refers to the maximum surface distance of two contacting aggregates [39,40]. If the surface distance is smaller than the SDT value, the two aggregates are assumed to be in contact, and the area captured by the SDT is regarded as CR. Thus, the effects of the aggregate contact characteristics on the TC asymmetry of AC can be assessed at the CR scale and further upgraded to the mesoscale modeling of AC with the help of CR [1].

2. Problem formulation

As aforementioned, the global TC asymmetry of AC may be associated with the local aggregate contact characteristics, but how aggregate contacts induce this asymmetric behavior has not been well understood yet and no available tool can be used to quantify this asymmetric behavior. Thus, this study aims to elucidate and quantify the micromechanical mechanisms of aggregate contact effect on AC's TC asymmetry. To achieve this objective, multiscale characterization and modeling at two length scales, including the microscale CR and mesoscale AC, were performed. Fig. 2 presents the research plan of this study, which includes two main tasks: 1) microscale characterization and modeling of the TC asymmetry of CR, and 2) mesoscale characterization and modeling of the TC asymmetry of AC.

In the first task, the nanoindentation measurement, which can identify material's microstructural and mechanical properties, such as elastic modulus, at the nanoscale level, was conducted to characterize the microscale aggregate contact characteristics in CR. Accordingly, the microstructural models of CR considering contact characteristics were developed. It is worth noting that asphalt mastic is the matrix phase in CR as identified from the nanoindentation test (Section 4.1). Thus, its viscoelastic properties were also measured and converted to Prony series for further modeling. Through the numerical modeling based on the developed CR model, the responses of CR in T&C could be predicted. Finally, to characterize the effect of aggregate contacts on the viscoelastic properties of CR in T&C, the predicted master curves were further assessed by the relaxation spectra and equilibrium moduli.

In the second task, the mesostructural model of AC incorporating CR was developed to account for aggregate contact effect. The

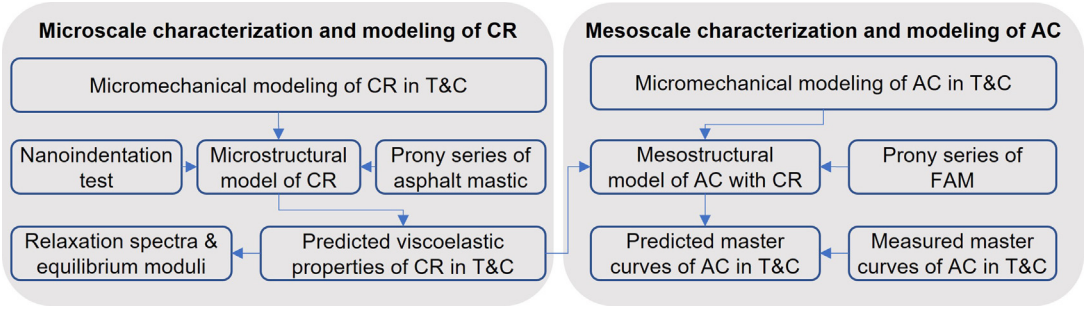

Fig. 2. Research plan of this study.

predicted CR properties based on the microscale CR model were applied to the CR phase in the developed AC model. Through numerical simulation, the mechanical performance of AC in T&C can be predicted. Meanwhile, the effective viscoelastic properties of AC were also characterized through laboratory tests. By comparing the testing and modeling results, the effect of aggregate contacts on AC's TC asymmetry can be quantified. In addition, it is worth mentioning that the matrix phase in AC model, i.e., FAM, may also show TC asymmetry, but its asymmetry may be much less significant than AC mixtures. This is because, different from the CR, the fine particles in FAM are dispersed in the asphalt mastic leading to much fewer aggregate contacts in FAM and hence less effect on FAM performance.

3. Theory background of viscoelasticity

It will be shown in Section 4.1 that CR is a composite of viscoelastic asphalt mastic and high modulus large-size filler particle and interfacial transition zone (ITZ). The asphalt mastic and the CR (in compression or tension only) can be assumed as LVE materials. The following constitutive relationship can describe their mechanical properties:

$$\sigma(t) = \int_0^t E(t-\tau)\frac{d\varepsilon(\tau)}{d\tau}d\tau \tag{1}$$

where t is time, and τ is a time variable of integration; and $E(t)$ is the relaxation modulus function in compression or tension. If the material is in shear, $G(t)$ will be utilized. The Poisson's ratio (υ) is assumed to be time-independent. Thus, the shear and bulk relaxation moduli can be derived as follows:

$$K(t) = \frac{E(t)}{3(1-2\upsilon)} \tag{2}$$

$$G(t) = \frac{E(t)}{2(1+\upsilon)} \tag{3}$$

$E(t)$ is a monotonically decreasing function and can be expressed as follows [41–43]:

$$E(t) = E_\infty + \int_{-\infty}^{\infty} h(t)e^{-t/\tau}dln\tau \tag{4}$$

where $h(t)$ is the relaxation spectrum and E_∞ is the long-term modulus or equilibrium modulus. Given the relaxation spectrum, $h(t)$, and the equilibrium modulus (E_∞), the LVE properties can be completely determined. Also, the LVE properties can be calculated by the relaxation spectrum in the frequency domain as follows [44]:

$$E'(\omega) = E_\infty + \int_{-\infty}^{\infty} h(\tau)\frac{\omega^2\tau^2}{1+\omega^2\tau^2}dln\tau \tag{5}$$

$$E''(\omega) = \int_{-\infty}^{\infty} h(\tau)\frac{\omega\tau}{1+\omega^2\tau^2}dln\tau \tag{6}$$

where E' and E'' denote the storage and loss moduli, respectively; ω is the angular frequency. Eqs. (5) and (6) indicate that if E' and E'' are known, $h(\tau)$ and E_∞ can be determined through optimization. For this purpose, the method proposed by Levenberg and Shah was adopted in this study to determine the $h(\tau)$ and E_∞ based on the E' and E'' values [45,46]. The following relaxation spectrum function is assumed:

$$h(\tau) = a_1 \times exp\left\{-a_2 \times [ln(\tau) - ln(a_3)]^2\right\} \tag{7}$$

where a_1, a_2, and a_3 are the parameters of the relaxation spectrum. In the logarithmic time scale, this function is a symmetrical bell-shaped curve, which can well describe the relaxation spectrum of asphalt materials, and the integration in Eqs. (5) and (6) can be achieved through numerical integration based on the trapezoidal rule [45]. In this study, the relaxation spectra and equilibrium moduli of CR were calculated to evaluate its viscoelastic characteristics. The E' and E'' of CR at different frequencies were predicted from its micromechanical model. By minimizing the difference of the predicted E' and E'' with the calculated ones from Eqs. (5) and (6), the $h(\tau)$ and E_∞ of CR can be determined.

Different from the continuous spectrum $h(\tau)$, if the integral in Eq. (4) is represented by the discrete approximation, $E(t)$ can be expressed by the discrete relaxation spectrum, as presented below:

$$E(t) = E_\infty + \sum_{i=1}^{N} h(\tau_i) \times \Delta ln\tau_i \times e^{-t/\tau_i} \tag{8}$$

$$E_i = h(\tau_i) \times \Delta ln\tau \tag{9}$$

where E_i is the discrete relaxation spectrum strength; Eq. (8) is also known as the Prony series model or generalized Maxwell model. In the frequency domain, Eq. (8) can be written as below:

$$E^*(\omega) = E'(\omega) + iE''(\omega) \tag{10}$$

$$E'(\omega) = E_\infty + \sum_{i=1}^{N} \frac{E_i\tau_i^2\omega^2}{1+\tau_i^2\omega^2} \tag{11}$$

$$E''(\omega) = \sum_{i=1}^{N} \frac{E_i\tau_i}{1+\tau_i^2\omega^2} \tag{12}$$

The Prony series model parameters can be determined by performing the regression analysis between the calculated values based on the constructed master curve and the predicted ones by minimizing the following objective function:

$$Objective\ function = \sum_{i=1}^{m}\left(\left(\frac{E'(\omega_i)_{pred}}{E'(\omega_i)_{cal}} - 1\right)^2 + \left(\frac{E''(\omega_i)_{pred}}{E''(\omega_i)_{cal}} - 1\right)^2\right) \tag{13}$$

where m is the total data points used; $E\prime(\omega_i)_{cal}$ and $E\prime\prime(\omega_i)_{cal}$ represent the calculated storage and loss modulus at the i^{th} frequency, respectively; and $E\prime(\omega_i)_{pred}$ and $E\prime\prime(\omega_i)_{pred}$ are the predicted storage and loss modulus at the i^{th} frequency based on the Prony series model parameters, respectively.

For the micromechanical modeling, the measured complex moduli of asphalt mastic were used to construct the master curves, which were then fitted by the Prony series model. The relaxation spectrum and equilibrium modulus introduced here were used to analyze the predicted viscoelastic properties of CR in T&C.

4. Laboratory test and results

4.1. Nanoindentation tests

Nanoindentation tests were conducted to characterize the contact characteristics of the CR between aggregates in contact. Preparing the nanoindentation sample can be summarized in three steps: sample cutting, epoxy resin casting, and polishing. A cylindrical sample with a diameter of 30 mm was first drilled out from the Marshall specimen and cut into 10 mm thin slices to fabricate the small pieces for the nanoindentation test. The slice sample was further embedded into epoxy resin for fixing. After 24-hour curing at room temperature, the top surface of the sample was polished. In this step, the specimen was ground by 180, 600, and 1200 grit SiC abrasive papers one by one and then polished by polishing cloths with successively finer polishing agents (9, 3, and 0.05 μm). The grinding and polishing processes took about two hours until the surface was thoroughly smooth. Finally, the specimen was cleaned in an ultrasonic bath with ethanol for 5 min. A root-mean-squared (RMS) roughness smaller than 50 nm could be achieved for the processed sample.

Fig. 3(a) presents the finished sample used in this study. A Bruker's Hysitron TI Premier Nano-indenter equipped with a scanning probe microscopy (SPM) was used to perform the nanoindentation test. In the test, a three-sided pyramidal diamond tip was used, and the indentation test was performed on the selected CR using the displacement-control mode, where the maximum indentation depth and spacing were 180 and 10 nm. Fig. 3(b) presents a CR between two aggregates on the test surface. It can be seen that the CR displays a sandwich-like structure, where large fine particles (at filler scale) are distributed in the narrow gap, and the remaining space is filled with asphalt mastic. The corresponding elastic modulus contour map of this CR is illustrated in Fig. 3(c). It is to be noted that the aggregate zone exhibits much higher moduli than the asphalt matrix region. A modulus of about 80 GPa was observed for the granitic aggregate. Besides, an interfacial transition zone (ITZ) layer with a thickness of around 10 μm and modulus of about 40 GPa along the aggregate peripheries was observed. The measured thickness is consistent with the observation in many previous studies, which is in the range between 5 and 25 μm [47]. Fig. 4 presents more captured CRs in AC mixtures through this test. It can be sensed that even for the same AC mixture, the morphology varies significantly due to the irregular aggregate surface. However, what can be confirmed is that the big aggregates are contacted via the large filler particles rather than full contact between the neighboring aggregate surfaces. The identified contact characteristics were subsequently utilized to develop the microstructural model of CR in Section 5.1.

4.2. Frequency sweep test

Frequency sweep tests were performed to measure the complex moduli of asphalt mastic, FAM, and AC mixture. Asphalt mastic is a mix of asphalt binder and mineral filler (<0.075 mm). FAM is composed of asphalt mastic and fine aggregates with sizes from 0.075 mm to 2.36 mm [48,49]. A dynamic shear rheometer (DSR) was used to conduct the frequency sweep test on asphalt mastic and FAM samples. The frequency sweep tests for AC in T&C were performed by a universal testing machine (UTM). The compressive frequency sweep tests were conducted following the AASHTO T342 by applying compressive sinusoidal loads considering different loading frequencies at different temperatures [50]. In the tensile test, tensile sinusoidal loads were applied. The measured complex moduli at different temperatures were then used to construct the master curves in a wider frequency range. Figs. 5 and 6 present the constructed master curves at a reference temperature of

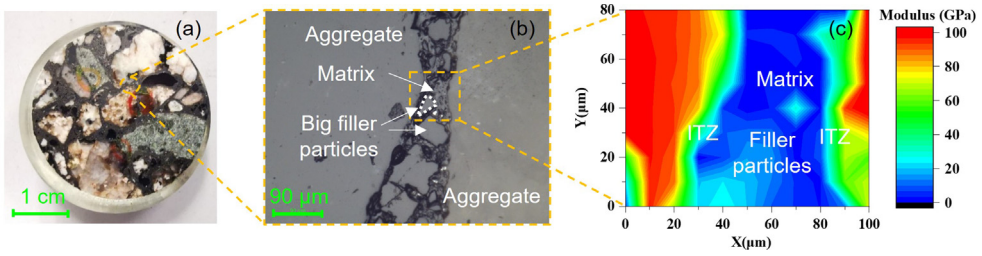

Fig. 3. Nanoindentation test: (a) Test sample; (b) Tested contact zone; and (c) Modulus contour map.

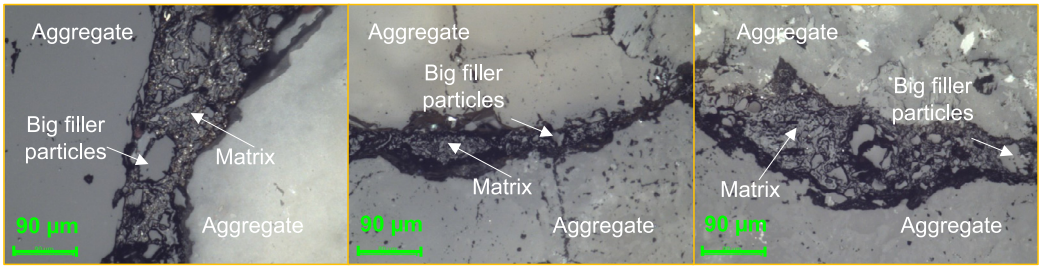

Fig. 4. CR images of SMA10 from the nanoindentation test.

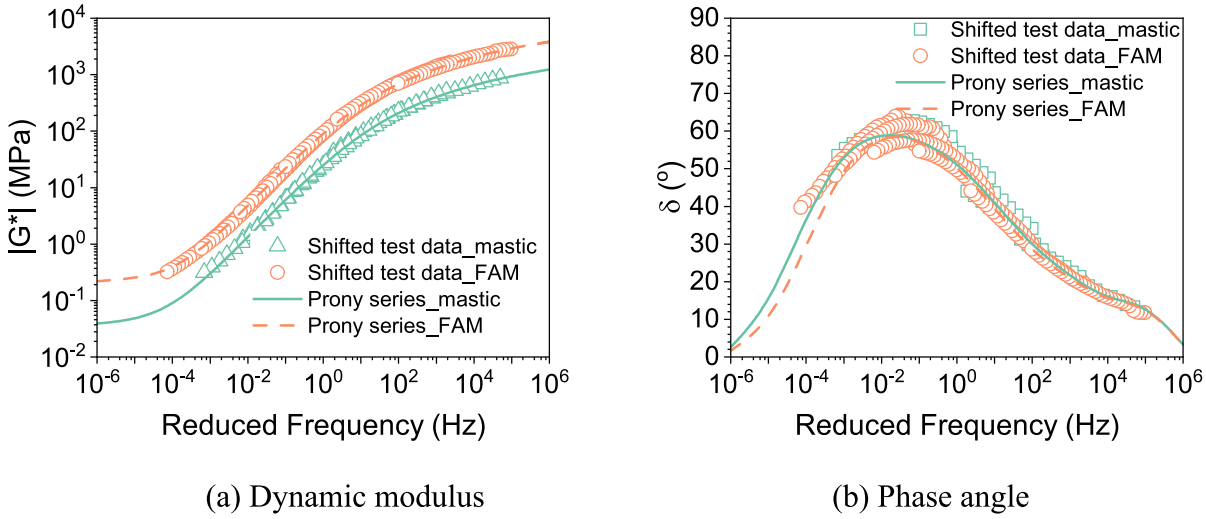

Fig. 5. Measured master curves of asphalt mastic and FAM of SMA10.

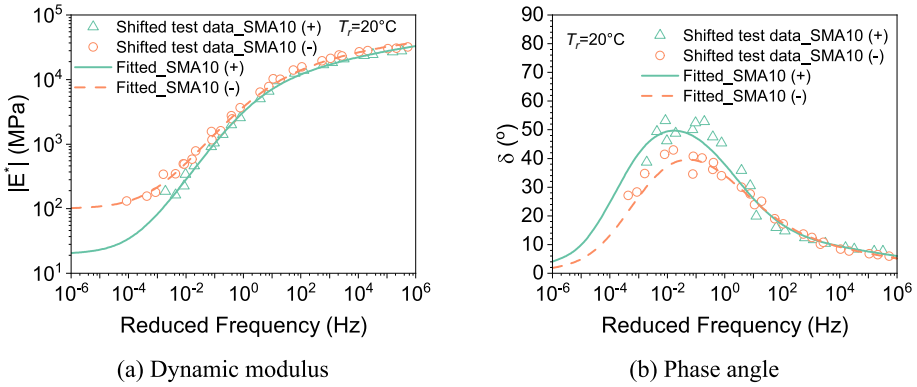

Fig. 6. Measured master curves of for AC in tension (+) and compression (−).

20 °C. The fitted Prony series models based on the measured master curves of asphalt mastic and FAM were used for numerical modeling. From Fig. 5, it can be seen that the optimized Prony-series models fit well with the tested master curves, which ensures the accuracy of the input data in the following numerical modeling. The measured master curves for AC in T&C were compared with the predicted ones. Fig. 6 shows that the AC mixture in tension shows lower dynamic moduli but higher phase angles than the ones in compression. This observation is consistent with the findings in previous studies [13,20,23].

5. Numerical model development and numerical computation

5.1. Micromechanical modeling of Contact region

Microstructural models of CR were developed based on the contact characteristics, as discussed in Section 4.1. As presented in Fig. 7(a-b), the generated CR model is an axisymmetric model, which can represent the 3D response based on the 2D model. The developed CR model comprises two ITZ layers, a large filler particle, and asphalt mastic. The large filler particle is located between the two ITZ layers with a thickness of 10 μm. The left zone is filled with asphalt mastic. The CR model's total height (H) is 0.1 mm, which was determined by the adopted SDT value of 0.1 mm, while the particle radius (R) is 0.04 mm, which was based on the maximum size of the filler particle: 0.075 mm in diameter. Since the contact point density in the CR was unclear, CR models with different lengths (L) were generated. The rate of model length to the radius of the fine particle, i.e., L/R, was utilized for representing the contact point density of CR. A lower L/R represents a higher contact point density. For the CR model in tension, zero-thickness cohesive elements were added on the surface of the fine particle to separate the element nodes between ITZ and the spherical particle. As presented in Fig. 7(c), an unbound material model without asphalt mastic was also developed to evaluate the aggregate contact effect on CR in compression. Numerical modeling was finally performed on the developed CR models with different (L/R) ratios to predict the viscoelastic properties of CR in T&C.

Table 1 presents the material properties utilized to develop the CR models. The ITZ and the larger filler particle were assumed as elastic materials with moduli of 80 and 40 MPa, respectively. The Prony series of asphalt mastic, obtained from laboratory tests as shown in Section 4.2, was applied to the matrix phase and cohesive zone elements in the developed CR model. In the T&C simulations for the CR, the bottom surface was fixed, and a compressive/tensile strain of 10^{-4} was introduced on the top surface. The steady-state dynamic (SSD) analysis was adopted to perform the dynamic simulation on CR in T&C. SSD method has been reported to be an efficient and accurate approach to conducting dynamic simulations [1,51].

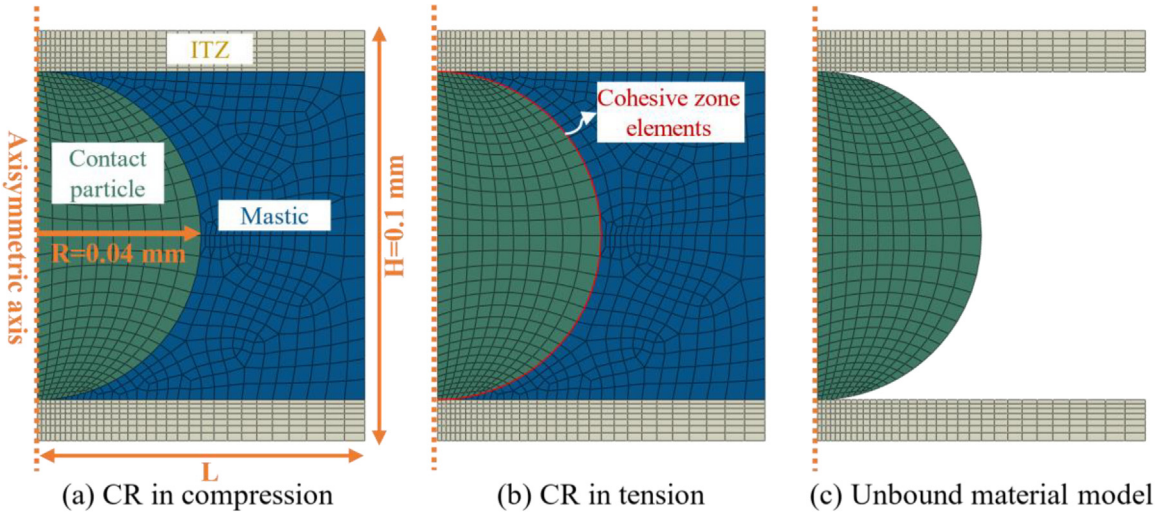

Fig. 7. Developed CR models.

Table 1
Material Properties.

Materials	Poisson's ratio	Elasticity/Viscoelasticity
Aggregate	0.2	80 GPa
ITZ	0.2	40 GPa
Asphalt mastic	0.45	Prony series model
FAM	0.4	Prony series model

5.2. Micromechanical modeling of AC

CT-based AC model was generated following the methodology proposed in [1]. The developed mesostructural AC model is composed of four phases: aggregate, matrix (FAM), CR and air void (empty zone). As shown in Fig. 8, developing the CT-based model can be summarized into three steps: image segmentation (Fig. 8 (b)), CR identification (Fig. 8(c)), and mesh model generation (Fig. 8(d)). In the step of CR identification, the regions between aggregate with an SDT value of 0.1 mm were recognized and identified as CRs. Based on the findings in our previous study [1], this value is suitable to account for all CRs in AC. The volumetric properties of the studied AC mixture, i.e., SMA10, are listed in Table 2. It can be found that the generated models have close volumetric compositions to the real specimen. Besides, it is noteworthy that CR only occupies a very tiny volumetric proportion in SMA10. The developed geometrical model was further meshed by the linear tetrahedral elements (C3D4) [1]. Fig. 8(d) displays the meshed AC model. In the generated mesh model, the void is empty. Aggregate, matrix and CR are assumed fully bonded. Thus, they share nodes at their interfaces. The cubic samples with 20 mm length for SMA10 were developed. Three replicates were generated, and the average element number of the developed models was 5.9 million.

The material properties used in the modeling are listed in Table 1. In the developed AC models, aggregates were regarded as elastic materials with Young's modulus and Poisson's ratio of 80 GPa and 0.2, respectively. The viscoelastic properties of the matrix, i.e., FAM, were described by the Prony series based on the measurement results presented in Fig. 5. The material properties of the CR phase were from the developed CR model, as shown in Section 5.2. The predicted tensile (compressive) viscoelastic properties were assigned to the CR phase in the AC model to

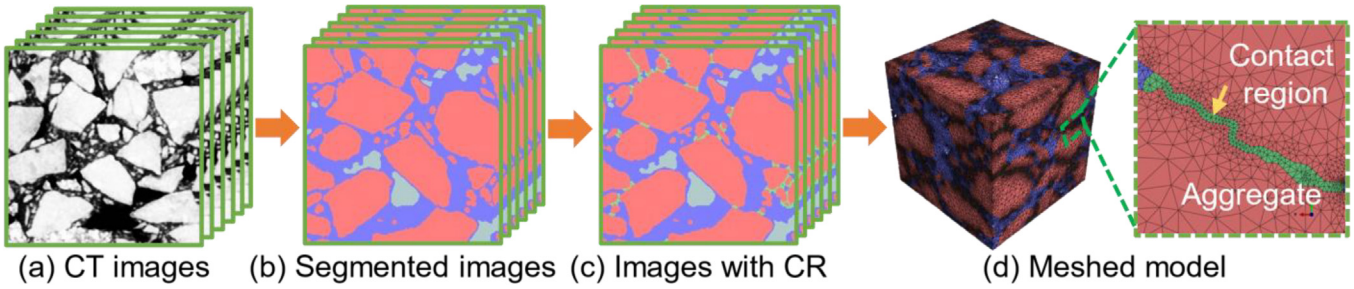

Fig. 8. CT model generation.

Table 2
Volumetric properties of the real asphalt mixture and the generated AC models (%).

Sample ID	Aggregate	Matrix	Air void	Contact region (CR)
Real SMA10 specimen	63.5	31.6	4.5	–
SMA10 model	62.5	31.7	4.3	1.5

predict the response of AC in tension (compression). Like the CR models, the bottom face of the developed AC model was fixed, and a 10^{-4} compressive/tensile strain was applied on the top surface. Then, the dynamic simulation based on SSD analysis was performed to predict the dynamic behavior of AC in T&C in the frequency range of 10^{-6} Hz to 10^{6} Hz. More details, such as the AC model generation, numerical convergence and computational cost, can be referred to our previous study [1].

6. Results and discussion

In this section, the predicted master curves of CR at different L/R values are first presented to evaluate the effect of contact characteristics on the viscoelastic properties of CR. Then, the stress distributions of CR, which can provide a more intuitive way to perceive the mechanical response of CR, are discussed. To correlate the microstructural characteristics of CR to its mechanical performance, the predicted master curves in the frequency domain were converted to relaxation spectra and equilibrium moduli in the time domain. In addition, parametric studies were performed to determine the appropriate L/R value of CR through the AC model in compression. Further, the determined CR properties in T&C were used to predict the master curve for the AC mixture. For simplicity, the '+' and '-' signs are utilized for representing the model in tension and compression, respectively.

6.1. Master curves of CR

Fig. 9 illustrates the predicted master curves of CR at L/R values ranging from one to five. It can be clearly observed that at both loading modes of in compression (Fig. 9(a-b)) and in tension (Fig. 9(c-d)), the CR can be significantly stiffened with decreasing L/R values by showing higher dynamic moduli and lower phase angles. These results are reasonable since a low L/R value represents a high contact point density. Besides, compared with asphalt mastic, significant improvement in the stiffness value can be found for the CR in both T&C. However, the corresponding increase is much more substantial in compression than in tension. Taking the CR model with L/R = 2 as an example, the dynamic modulus of CR at 10^{-6} Hz is 31.5 MPa in compression, but only 2.5 MPa in tension. Such significant differences can be attributed to the contact characteristics, which will be further discussed in Section 6.2 and Section 6.3.

6.2. Stress distributions of CR

The stress distributions in CR models at L/R = 2 were evaluated to analyze the stress characteristics of CR. Fig. 10 presents the principal stress contour maps of CR in T&C at two frequencies (10^{-6} Hz and 10^{6} Hz). It can be found that high stress resides in the contact areas between ITZ layers and the large filler particle for CR in both compression (Fig. 10(a) and (c)) and tension (Fig. 10(b) and (d)), indicating that the touching area is critical to CR's load transmission. Comparing the stress distributions at different loading modes, it can be observed that at 10^{-6} Hz, CR in compression (Fig. 10(a)) shows much higher stress in tension (Fig. 10(b)), indicating that the large filler particle served as contact points can dramatically improve the stress transmission between touching aggregates at the low frequency, while at 10^{6} Hz, although the stress for CR in compression (Fig. 10(c)) is still higher than CR in tension (Fig. 10(d)), the discrepancy was found to be significantly reduced. It can be inferred that with increasing frequency, the stiffening asphalt mastic improves stress transmission between ITZ layers and thus dwarfs the effects of aggregate contacts in the CR.

6.3. Relaxation spectra and equilibrium moduli of CR

The relaxation spectra and equilibrium modulus of CR were utilized to assess the viscoelastic properties of CR in T&C. Similar to the dynamic modulus and phase angle in the frequency domain,

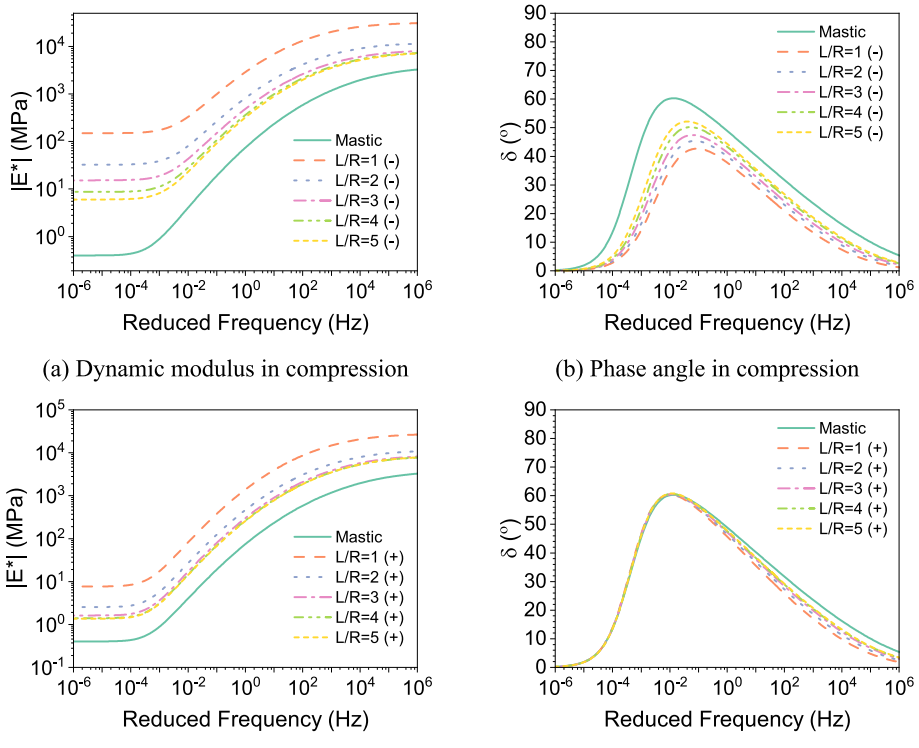

(a) Dynamic modulus in compression

(b) Phase angle in compression

(c) Dynamic modulus in tension

(d) Phase angle in tension

Fig. 9. Predicted master curves of CR in compression/tension at different L/R values.

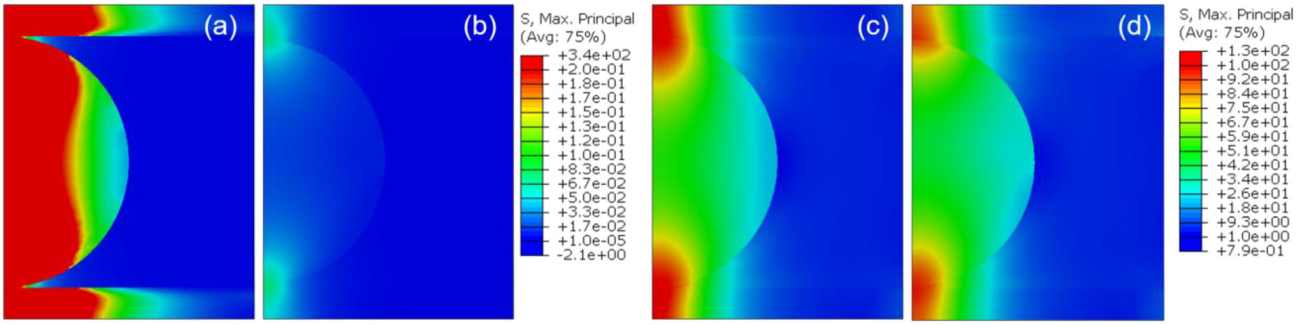

Fig. 10. Principal stress distribution in CR models at L/R = 2: (a) In compression at 10^{-6} Hz; (b) In tension at 10^{-6} Hz; (c) In compression at 10^{6} Hz; and (d) In tension at 10^{6} Hz.

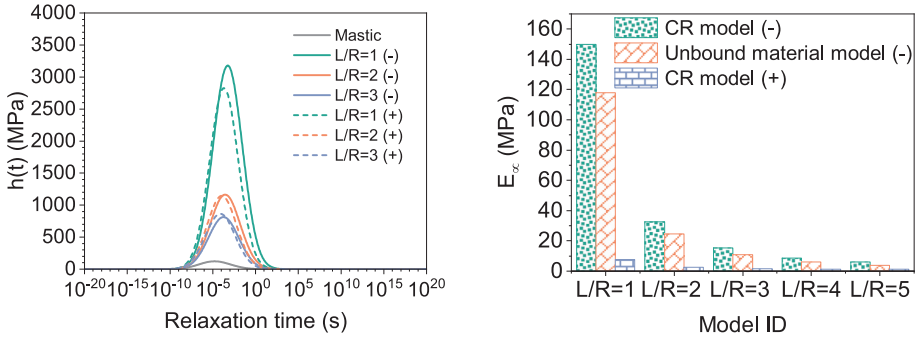

(a) Relaxation spectra (b) Equilibrium moduli

Fig. 11. Relaxation spectra and equilibrium moduli of CR.

viscoelastic properties can also be entirely represented by the relaxation spectrum and equilibrium modulus in the time domain, as indicated in Eq. (5) to Eq. (7). MATLAB codes were developed to perform numerical integration to convert the predicted master curves of dynamic modulus and phase angle as shown in Fig. 9 to relaxation spectra and equilibrium moduli [45]. The built-in 'fmincon' function was adopted to optimize $h(\tau)$ and E_∞ by minimizing the difference between the calculated E' and E'' (Eqs. (5) and Eq. (7)), and the corresponding predicted values from the micromechanical model of CR. Fig. 11(a) presents the relaxation spectra of CR at different L/R values. It is to be noted that, at the same L/R value, the difference in the relaxation spectra for CR in T&C is insignificant. Besides, compared with the relaxation spectrum of asphalt mastic, the relaxation spectra of CR are significantly higher within the relaxation time from 10^{-8} to 10^{3} s and increase with increasing contact point density (decreasing L/R value). Such an improvement indicates that the relaxation spectrum mainly reflects the particle filling effect. As illustrated in Fig. 12, compared with the model of CR without particle, the filler particle in the models of CR in T&C replaces part of the asphalt matrix and thus makes the CR stiffer. Besides, a higher contact point density (lower L/R value) represents the larger volumetric replacement and thus leads to the higher relaxation spectra for CR in T&C. Fig. 11(b) displays the equilibrium moduli of CR. Also, the moduli from the unbound material model (without matrix) were plotted to evaluate the contribution of the aggregate contact only. It can be seen that the equilibrium moduli in compression are much higher than in tension but close to the predicted moduli from the unbound material model. This result demonstrates that the aggregate contact effect dictates the equilibrium modulus of CR in compression. As shown in Fig. 13, the stiff contact point can significantly improve the stress transmission between ITZ layers for the CR and the unbound material models in compression, but cannot play its role for CR in tension. Thus, the equilibrium modulus of CR in compression is much larger than in tension.

6.4. Master curves of AC

To determine the viscoelastic properties of CR material, the appropriate L/R value for the proposed CR model in Section 5.1 should be determined. For this purpose, CR models at three L/R values of 2.0, 2.5, and 3.0 were selected to predict the viscoelastic properties of CR, which were further applied to the developed AC model for predicting the master curves of AC mixture at different contact properties. Fig. 14 presents the predicted master curves of SMA10 in compression mode. The measured master curves from the laboratory test under the compression mode were also plotted. The higher dynamic moduli and lower phase angles with decreasing L/R value (increasing contact point density) indicate higher elasticity of AC mixtures in compression. Besides, it can be found that among the three L/R values, the predicted master curves based on the CR model at L/R = 2.5 best agree with the experimental ones, indicating an L/R value of 2.5 may be suitable for SMA10. Thus, L/R equal to 2.5 was adopted to predict the complex moduli for AC in T&C.

Fig. 15 presents the predicted master curve of AC in T&C. It can be observed that the predicted master curves in T&C agree well with the experimental ones, indicating that the developed model can reasonably predict the mechanical performance of AC. At low frequencies, significantly higher compressive moduli than tensile ones were found. For example, at 10^{-6} Hz, the compressive modulus is around six times higher than the tensile modulus. Besides,

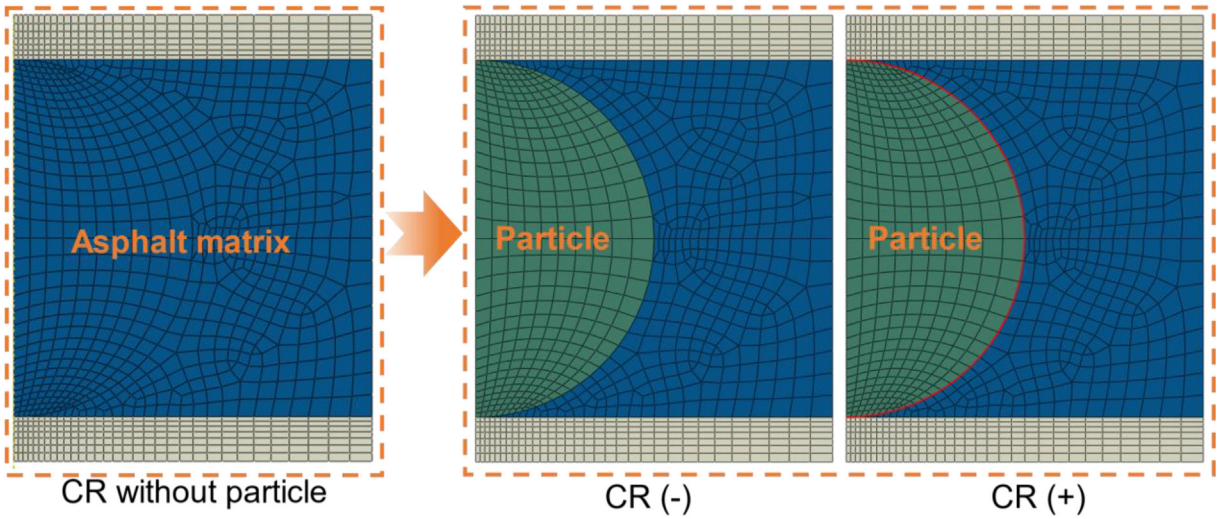

Fig. 12. Particle filling effect.

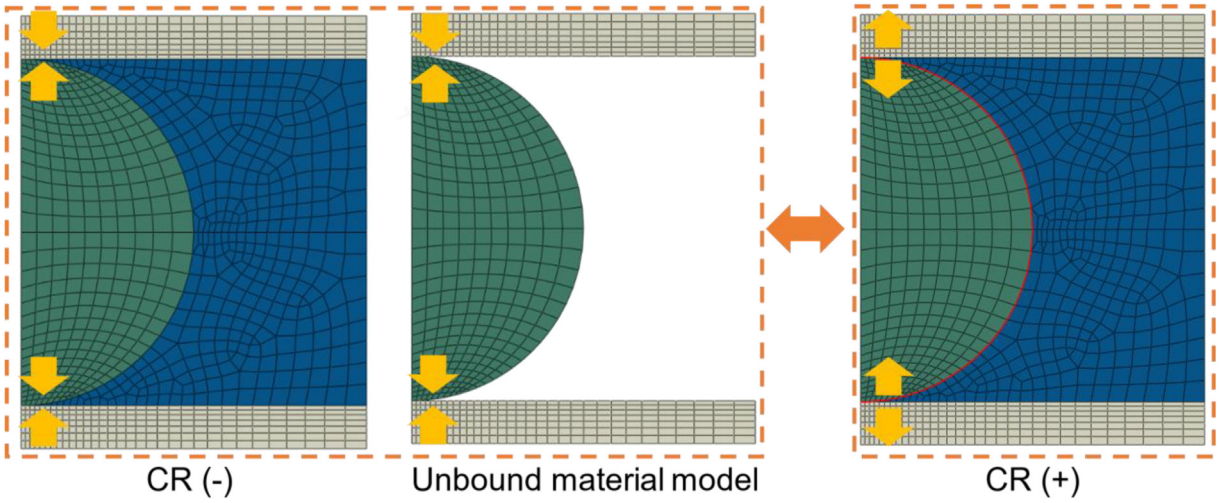

Fig. 13. Aggregate contact effect.

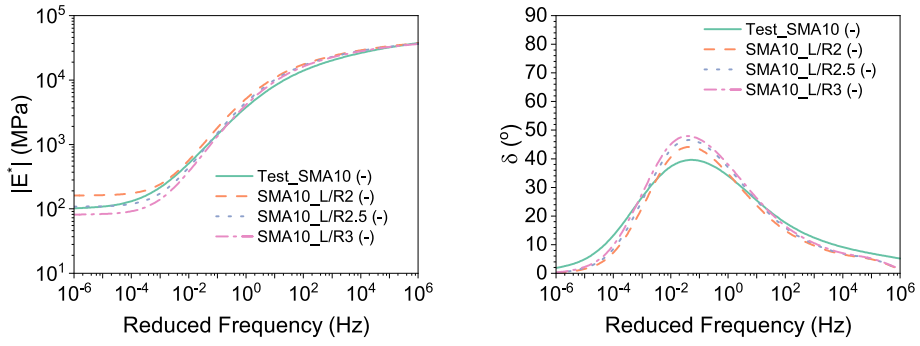

(a) Dynamic modulus (b) Phase angle

Fig. 14. Predicted master curves of AC in compression at different L/R values.

the peak tensile phase angles are 31% higher than the corresponding value under compression mode. These significant disparities for AC in T&C demonstrated the considerable effect of CR in the TC asymmetry of AC. From a multiscale view, the unique microstructure of CR causes the microscale asymmetric performance of CR in T&C and further leads to the mesoscale TC asymmetry of AC. Besides, it can be found that the master curves in T&C converge with the increase in frequency. This performance may be explained by the viscoelasticity of asphalt materials. At low frequencies, the FAM and CR phases in the AC model exhibit more

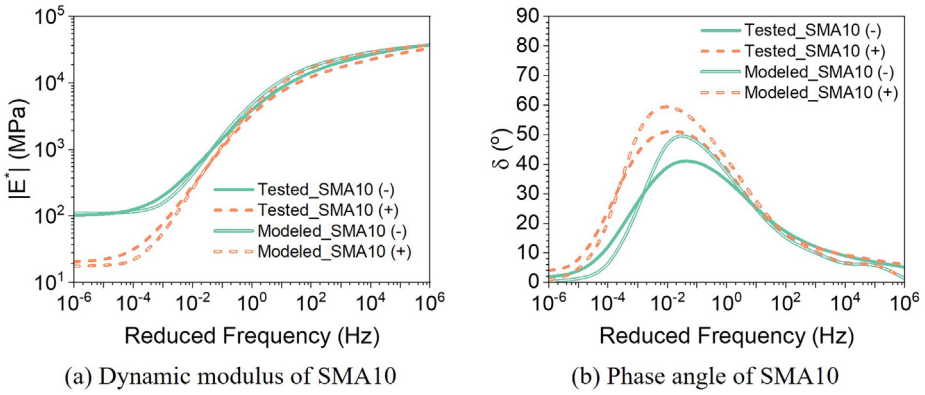

(a) Dynamic modulus of SMA10 (b) Phase angle of SMA10

Fig. 15. Predicted master curves of SMA10 in compression and tension at R/L = 2.5.

viscous behavior and thus leading to a lower modulus. With the increase of frequencies, the asphalt matrix and CR become more elastic and thus reducing the aggregate contact effect.

7. Findings and conclusions

T&C asymmetry refers to the disparity in mechanical performance for AC in tension and compression. In this study, the underlying mechanisms of aggregate contact effect on this behavior were explored and quantified through multiscale characterization and modeling. Nanoindentation tests were performed to characterize the contact microstructural properties between aggregates. The corresponding microstructural model of CR was developed to evaluate the aggregate contact effect on the mechanical behavior of CR. Furthermore, the viscoelastic properties of CR in T&C were expressed by the time domain's relaxation spectrum and equilibrium modulus. Finally, the predicted CR properties were applied to the developed mesostructural model of the AC mixture to quantify the aggregate contact effect on the viscoelastic properties of AC in T&C. Based on the results from this study, the following findings can be obtained:

(1) Microscopically, CR is a sandwich-like structure composed of two stiffened ITZ layers, asphalt mastic and large filler particles, in which the large filler particles play the role of contact points.

(2) CR exhibits significant TC asymmetry. CR in compression shows much higher dynamic moduli and lower phase angles than CR in tension, especially at low frequencies (high temperatures). A higher contact point density, i.e., lower L/R value, gives CR the larger compressive moduli and thus leads to more significant TC asymmetry.

(3) The unique contact characteristics lead to the disparity of CR in T&C. The particle filling effect determines the relaxation spectrum of CR regardless of loading modes (in tension/compression), and the aggregate contact effect dictates the equilibrium modulus of CR in compression. A high contact point density leads to a higher relaxation spectrum and equilibrium modulus.

(4) AC's TC asymmetry was quantified through the developed mesostructural AC model with CR. The predicted master curves in T&C are in quantitative agreement with experimental results indicating that the proposed modeling approaches can accurately predict the viscoelastic properties of AC mixtures in T&C.

Through multiscale characterization and numerical modeling, this study quantified the effects of aggregate contact characteristics on the asymmetric performance of AC in T&C. The unique aggregate contact characteristics cause the microscale disparity of CR in T&C and further lead to the macroscale TC asymmetry of AC. Based on the findings in this study, it can be concluded that aggregate contacts are one of the primary factors that cause the asymmetric performance of AC. To our best knowledge, this is the first study to quantify the effects of aggregate contacts on the asymmetric performance of AC. The outcomes of this study can be further applied to evaluate the effects of TC asymmetry on different performance properties of asphalt pavement.

CRediT authorship contribution statement

Zhifei Tan: Conceptualization, Software, Investigation, Writing – original draft. **Bin Yang:** Investigation, Validation. **Zhen Leng:** Supervision, Methodology, Funding acquisition, Writing – review & editing. **Denis Jelagin:** Supervision, Conceptualization, Writing – review & editing. **Peng Cao:** Software, Validation. **Rui Li:** Data curation, Writing – review & editing. **Fuliao Zou:** Data curation, Writing – review & editing.

Data availability

Data will be made available on request.

Declaration of Competing Interest

The authors declare that they have no known competing financial interests or personal relationships that could have appeared to influence the work reported in this paper.

Acknowledgments

The authors sincerely acknowledge the funding support from Hong Kong Research Grant Council through the GRF project 15204022.

References

[1] Z. Tan, Z. Leng, J. Jiang, P. Cao, D. Jelagin, G. Li, A. Sreeram, Numerical study of the aggregate contact effect on the complex modulus of asphalt concrete, Mater. Des. 213 (2022), https://doi.org/10.1016/j.matdes.2021.110342 110342.

[2] H. Fadil, D. Jelagin, P.-L. Larsson, M.N. Partl, Measurement of the viscoelastic properties of asphalt mortar and its components with indentation tests, Road Mater. Pavement Des. 20 (2019) S797–S811, https://doi.org/10.1080/14680629.2019.1628434.

[3] P. Cao, F. Jin, C. Zhou, D. Feng, Investigation on statistical characteristics of asphalt concrete dynamic moduli with random aggregate distribution model, Constr. Build. Mater. 148 (2017) 723–733, https://doi.org/10.1016/j.conbuildmat.2017.05.012.

[4] N.C.H.R. Program (NCHRP), Guide for mechanistic-empirical design of new and rehabilitated pavement structures, Transportation Research Board, Washington, DC, 2004.

[5] M.K. Darabi, R.K. Abu Al-Rub, E.A. Masad, C.-W. Huang, D.N. Little, A modified viscoplastic model to predict the permanent deformation of asphaltic

materials under cyclic-compression loading at high temperatures, Int. J. Plast. 35 (2012) 100–134, https://doi.org/10.1016/j.ijplas.2012.03.001.
[6] C.-W. Huang, R.K. Abu Al-Rub, E.A. Masad, D.N. Little, Three-dimensional simulations of asphalt pavement permanent deformation using a nonlinear viscoelastic and viscoplastic model, J. Mater. Civ. Eng. 23 (1) (2011) 56–68.
[7] E. Levenberg, J. Uzan, Triaxial small-strain viscoelastic-viscoplastic modeling of asphalt aggregate mixes, Mech. Time-Depend. Mater. 8 (2004) 365–384, https://doi.org/10.1007/s11043-004-1592-1.
[8] Z. Zhang, M. Oeser, Residual strength model and cumulative damage characterization of asphalt mixture subjected to repeated loading, Int. J. Fatigue (2020), https://doi.org/10.1016/j.ijfatigue.2020.105534 105534.
[9] B.B. Yin, W.K. Sun, Y. Zhang, K.M. Liew, Modeling via peridynamics for large deformation and progressive fracture of hyperelastic materials, Comput. Methods Appl. Mech. Eng. 403 (2023) 115739.
[10] B.B. Yin, A. Akbar, Y. Zhang, K.M. Liew, Modeling progressive failure and crack evolution in a randomly distributed fiber system via a coupled phase-field cohesive model, Compos. Struct. 313 (2023) 116959.
[11] J. Kollmann, G. Lu, P. Liu, Q. Xing, D. Wang, M. Oeser, S. Leischner, Parameter optimisation of a 2D finite element model to investigate the microstructural fracture behaviour of asphalt mixtures, Theor. Appl. Fract. Mech. 103 (2019), https://doi.org/10.1016/j.tafmec.2019.102319 102319.
[12] S.W. Katicha, G.W. Flintsch, A. Loulizi, Bimodular analysis of hot-mix asphalt, Road Mater. Pavement Des. 11 (2010) 917–946, https://doi.org/10.1080/14680629.2010.9690313.
[13] P. Khanal, M. Mamlouk, Tensile versus compressive moduli of asphalt concrete, Transp. Res. Rec. 144–150 (1995).
[14] C.L. Monismith, K.E. Secor, Viscoelastic behavior of asphalt concrete pavements, in: Ann Arbor, Michigan, 1962: pp. 728–760.
[15] Q.T. Nguyen, H. Di Benedetto, C. Sauzéat, M.L. Nguyen, T.T.N. Hoang, 3D complex modulus tests on bituminous mixture with sinusoidal loadings in tension and/or compression, Mater. Struct. 50 (2016) 98, https://doi.org/10.1617/s11527-016-0970-x.
[16] K.S. Pister, R.A. Westmann, Analysis of viscoelastic pavements subjected to moving loads, in: Int. Conf. Struct. Des. Asph. Pavements, Ann Arbor, Michigan, 1962.
[17] Z. Dai, V. Laheri, X. Zhu, F.A. Gilabert, Experimental study of compression-tension asymmetry in asphalt matrix under quasi-static and dynamic loads via an integrated DMA-based approach, Constr. Build. Mater. 283 (2021), https://doi.org/10.1016/j.conbuildmat.2021.122725 122725.
[18] B. Keshavarzi, Y.R. Kim, A viscoelastic-based model for predicting the strength of asphalt concrete in direct tension, Constr. Build. Mater. 122 (2016) 721–727, https://doi.org/10.1016/j.conbuildmat.2016.06.089.
[19] S. Lv, C. Liu, H. Yao, J. Zheng, Comparisons of synchronous measurement methods on various moduli of asphalt mixtures, Constr. Build. Mater. 158 (2018) 1035–1045, https://doi.org/10.1016/j.conbuildmat.2017.09.193.
[20] R.L. Lytton, F. Gu, Y. Zhang, X. Luo, Characteristics of undamaged asphalt mixtures in tension and compression, Int. J. Pavement Eng. 19 (2018) 192–204, https://doi.org/10.1080/10298436.2017.1279489.
[21] Y. Zhang, R. Luo, R.L. Lytton, Anisotropic viscoelastic properties of undamaged asphalt mixtures, J. Transp. Eng. 138 (2012) 75–89, https://doi.org/10.1061/(ASCE)TE.1943-5436.0000302.
[22] E.R. Hargett, E.E. Johnson, Strength properties of bituminous concrete tested in tension and compression, Highw. Res. Board ProC, 1961.
[23] H. Cheng, Y. Wang, L. Liu, L. Sun, Y. Zhang, R. Yang, Estimating tensile and compressive moduli of asphalt mixture from indirect tensile and four-point bending tests, J. Mater. Civ. Eng. 33 (2021) 04020402, https://doi.org/10.1061/(ASCE)MT.1943-5533.0003476.
[24] E. Levenberg, Viscoelastic tension-compression nonlinearity in asphalt concrete, J. Mater. Civ. Eng. 27 (2015) 04015048, https://doi.org/10.1061/(ASCE)MT.1943-5533.0001319.
[25] R.L. Lytton, J. Uzan, E.G. Fernando, R. Roque, D. Hiltunen, S.M. Stoffels, Development and validation of performance prediction models and specifications for asphalt binders and paving mixes, Strategic Highway Research Program, Washington, DC, United States, 1993. https://trid.trb.org/view/388773 (accessed December 25, 2021).
[26] X. Cai, Z. Leng, P. Kumar Ashish, J. Yang, M. Gong, Quantitative analysis of the role of temperature in the mesoscale damage process of semi flexible pavement composite through finite element method, Theor. Appl. Fract. Mech. 124 (2023), https://doi.org/10.1016/j.tafmec.2022.103742 103742.
[27] J. Jiang, Z. Leng, B. Yang, G. Lu, Z. Tan, M. Han, Z. Dong, Penetration mechanism of the emulsion-based rejuvenator in damaged porous asphalt mixture: Microstructure characterization and 3D reconstruction, Mater. Des. 221 (2022), https://doi.org/10.1016/j.matdes.2022.111014 111014.
[28] X. Shu, B. Huang, Dynamic modulus prediction of HMA mixtures based on the viscoelastic micromechanical model, J. Mater. Civ. Eng. 20 (2008) 530–538, https://doi.org/10.1061/(ASCE)0899-1561(2008)20:8(530).
[29] B.S. Underwood, Y.R. Kim, Microstructural association model for upscaling prediction of asphalt concrete dynamic modulus, J. Mater. Civ. Eng. 25 (2013) 1153–1161, https://doi.org/10.1061/(ASCE)MT.1943-5533.0000657.
[30] E. Masad, M.E. Kutay, Characterization of the internal structure of asphalt mixtures, Appl. Adv. Models Understand Behav Perform. Asph. Transp. Res. E-Circ. (2012) 2–16.
[31] P. Polaczyk, Y. Ma, Z. Jarrar, X. Jiang, R. Xiao, B. Huang, Quantification of asphalt mixture interlocking utilizing 2D and 3D image processing, J. Mater. Civ. Eng. 35 (2023) 04022382, https://doi.org/10.1061/(ASCE)MT.1943-5533.0004560.
[32] J. Jiang, F. Ni, L. Gao, L. Yao, Effect of the contact structure characteristics on rutting performance in asphalt mixtures using 2D imaging analysis, Constr. Build. Mater. 136 (2017) 426–435, https://doi.org/10.1016/j.conbuildmat.2016.12.210.
[33] Y. Sun, J. Chen, B. Pan, X. Shu, B. Huang, Three-dimensional micromechanical complex-modulus prediction of asphalt concrete considering the aggregate interlocking effect, J. Mater. Civ. Eng. 29 (2017) 04017153, https://doi.org/10.1061/(ASCE)MT.1943-5533.0001997.
[34] H. Zhang, K. Anupam, T. Scarpas, C. Kasbergen, S. Erkens, Contact mechanics based solution to predict modulus of asphalt materials with high porosities, Mater. Des. (2021), https://doi.org/10.1016/j.matdes.2021.109752 109752.
[35] C. Du, P. Liu, M. Oeser, Homogenization of the elastic-viscoplastic damage behavior of asphalt mixtures based on the mesomechanical Mori-Tanaka method, Eng. Comput. (2022), https://doi.org/10.1007/s00366-022-01628-3.
[36] P. Cao, Z. Leng, F. Shi, C. Zhou, Z. Tan, Z. Wang, A novel visco-elastic damage model for asphalt concrete and its numerical implementation, Constr. Build. Mater. 264 (2020), https://doi.org/10.1016/j.conbuildmat.2020.120261 120261.
[37] W. Song, F. Xu, H. Wu, Z. Xu, Investigating the skeleton behaviors of open-graded friction course using discrete element method, Powder Technol. 385 (2021) 528–536, https://doi.org/10.1016/j.powtec.2021.03.012.
[38] J. Xu, C. Xu, R. Wang, C. Jiang, S. Jiao, M. Hyodo, Microscopic mechanism analysis of influence of high effective confining pressure on mechanical properties of hydrate-bearing sediments, Comput. Geotech. 152 (2022), https://doi.org/10.1016/j.compgeo.2022.105011 105011.
[39] A.R. Coenen, M.E. Kutay, N.R. Sefidmazgi, H.U. Bahia, Aggregate structure characterisation of asphalt mixtures using two-dimensional image analysis, Road Mater. Pavement Des. 13 (2012) 433–454, https://doi.org/10.1080/14680629.2012.711923.
[40] M.E. Kutay, E. Arambula, N. Gibson, J. Youtcheff, Three-dimensional image processing methods to identify and characterise aggregates in compacted asphalt mixtures, Int. J. Pavement Eng. 11 (2010) 511–528, https://doi.org/10.1080/10298431003749725.
[41] R.S. Lakes, Viscoelastic solids, CRC Press, 1998.
[42] K.S. Cho, Viscoelasticity of polymers, Springer, Netherlands, Dordrecht (2016), https://doi.org/10.1007/978-94-017-7564-9.
[43] N.W. Tschoegl, The phenomenological theory of linear viscoelastic behavior, Springer, Berlin Heidelberg, Berlin, Heidelberg (1989), https://doi.org/10.1007/978-3-642-73602-5.
[44] J.D. Ferry, Viscoelastic Properties of Polymers, John Wiley & Sons, 1980.
[45] E. Levenberg, A. Shah, Interpretation of complex modulus test results for asphalt-aggregate mixes, J. Test. Eval. 36 (2008), https://doi.org/10.1520/JTE101577 101577.
[46] E. Levenberg, Smoothing asphalt concrete complex modulus test data, J. Mater. Civ. Eng. 23 (2011) 606–611, https://doi.org/10.1061/(ASCE)MT.1943-5533.0000217.
[47] X. Zhu, Y. Yuan, L. Li, Y. Du, F. Li, Identification of interfacial transition zone in asphalt concrete based on nano-scale metrology techniques, Mater. Des. 129 (2017) 91–102, https://doi.org/10.1016/j.matdes.2017.05.015.
[48] Z. Leng, Z. Tan, P. Cao, Y. Zhang, An efficient model for predicting the dynamic performance of fine aggregate matrix, Comput. Civ. Infrastruct. Eng. 36 (11) (2021) 1467–1479.
[49] Y. Zhang, Z. Leng, Quantification of bituminous mortar ageing and its application in ravelling evaluation of porous asphalt wearing courses, Mater. Des. 119 (2017) 1–11, https://doi.org/10.1016/j.matdes.2017.01.052.
[50] AASHTO T 342 Standard method of test for determining dynamic modulus of hot mix asphalt (HMA), (2019).
[51] P. Cao, F. Jin, C. Zhou, D. Feng, W. Song, Steady-state dynamic method: An efficient and effective way to predict dynamic modulus of asphalt concrete, Constr. Build. Mater. 111 (2016) 54–62, https://doi.org/10.1016/j.conbuildmat.2016.02.071.